

The characteristics of the Mocoa compound disaster event, Colombia

Abstract A rainfall-induced compound disaster happened in Mocoa in the pre-dawn hours of 1 April 2017. More than 300 people were killed, and a large number of houses and roads were destroyed in the worst catastrophe in the history of Mocoa. To investigate this disaster, a detailed interpretation was carried out using high-resolution images. Analysis of disaster characteristics based on satellite image revealed that the disaster could be identified as a consequence of compound mountain hazards including landslides, debris flows, and mountain torrents. The mountain hazards converged in the mountain watershed, which amplified the disaster's effects. Analysis considers that this disaster is the result of heavy rainfalls. Moreover, in-depth interpretation of rainfall data and satellite images spanning over 16 years reveals that the previous El Niño event (2014–2016) also played an important role, which caused reduced rainfall and vegetation coverage. The long period of drought brought by El Niño affected the growth of vegetation and reduced the ability of vegetation to cope with heavy rainfalls. The results reveal that both antecedent rainfalls and climate impact need to be taken into consideration for mountain hazard analysis.

Keywords Compound mountain hazards · Tropical alpine area · El Niño · Rainfall · Vegetation coverage · Debris flow

Introduction

Mountain torrents, landslides, and debris flows are common mountain hazards. There are many causes of mountain hazards, such as earthquakes (Chen et al., 2011a), rainfalls (Zhou et al. 2013; Cui et al. 2017), freeze-thaw (Wang and Yong 2008), river erosion (Lévy et al. 2012), vegetation reduction (Runyan and D'odorico 2014), slope instability (Dai and Lee 2002), and human activities (Preuth et al. 2010). When heavy rainfalls occur in the mountains, mountain hazards such as landslide (Iverson 2000, Zhou et al. 2016), mountain torrents (Eisbacher 1982), and debris flows (Ge et al. 2014) may be induced. These hazards could destroy settlements, block rivers, and bury farms and forests, causing huge casualties, property loss, and damage to the ecological environment (Cui 2014). In different mountain hazard cases, the causal factors that affect mountain hazards may be diverse because of the unique geographical environment of different regions.

Mocoa (76° 38' 49" W, 1° 8' 54" N), the capital of Putumayo province in Colombia, is located in the Andes Mountains (Fig. 1(a)) and is characterized by tropical-mountain weather with high-intensity rainfall (Sillitoe et al. 1984). Heavy rainfall starting from 11:00 p.m. on 31 March 2017 caused overflows in the rivers (Rio Mocoa, Rio Sangoyaco, Rio Mulata, and several others) (Fig. 1(b)) during the pre-dawn hours of 1 April 2017. Landslides occurring in the catchment of the Quebrada Taruca River and river erosion provided massive debris for river floods. As a result, the coupling of floods and mass debris evolved into debris flows downstream in the Taruca ravine, northwest of Mocoa. The floods and debris flows at speeds of 56–64 km/h (Hughes 2017) rushed resident

buildings, streets, bridges, and other infrastructures (Guardian 2017; Semana 2017). Massive debris and mud piled up in the city, with tree limbs, rocks, fencing, and vehicles in a disorderly mix (Fig. 1(c, d)). This disaster resulted in 316 dead, 332 injured, and 103 missing (Reliefweb 2017), and affected 17 neighborhoods of the city and approximately 45,000 people (ABC News 2017).

The increased frequency and magnitude of extreme weather events is becoming one of the major causes of disasters (Yilmaz 2017). Rainfalls were an important causal factor in the Mocoa disaster events. This study aims to comprehend the disaster characteristics and the hazard causal factors. An in-depth analysis of the disaster events of mountain hazards is helpful to understand the causes and effects of disasters and provide lessons for disaster prevention and mitigation in the process of mountain society development. This study shows that in the region's rainfall-induced mountain hazards, early drought events caused by the El Niño event that could affect rainfalls and vegetation should also be taken into account while studying antecedent rainfalls.

Watershed background and data source

Watershed background

The Shuttle Radar Topography Mission (SRTM) Digital Elevation Model (DEM) data with 30-m resolution were obtained from the USGS (Yang 2011, USGS 2017). Using watershed extraction method (ArcGIS Help 2012), the Mocoa watershed boundaries were obtained based on the DEM data. Mocoa is located in the lower right corner (Fig. 2(a)). This watershed has a complex geological environment (Fig. 2(b)), and the lithology near the city is the Mesozoic Plutonic rock (OneGeology 2007). Located on the east side of the Andes, the watershed's elevation ranges from 535 to 3606 m (Fig. 2(c)). Mocoa lies in a lower eastern valley. The slope gradients of this area range from 0° to 76.23° (Fig. 2(d)). Slope areas of 15° to 45° where landslides could occur have the largest percentage, occupying 78.21% of the area. There are three main climate types (Peel et al. 2007) in this watershed, including the Af (rainforest) climate type, the Cfb (oceanic) climate type, and the ET (tundra) climate type (Fig. 2(e)) (Fick and Hijmans 2017). The vegetation coverage of 2017 before the Mocoa disaster occurred (Fig. 2(f)) was calculated using MODIS normalized difference vegetation index (NDVI) products named by MOD13Q1. Using the maximum value composite (MVC) method (Eidenshink and Faundeen 1994, Stow et al. 2004), vegetation coverages were calculated based on the NDVI data (NASA 2017) and the dimidiate pixel model (Cui et al. 2011). The pixel cumulative percentages of 0.5% and 99.5% were selected as confidence intervals. In this basin, 19.93% of the total area has 60 to 80% vegetation cover, while 66.58% of the total area has 80 to 100% vegetation cover.

The hypsometric integral (HI) is a quantitative index to study the relationship between the horizontal section area and its elevation. HI could reflect the landform erosion stage and evolution process (Zhu et al. 2013). Strahler (1952) divided geomorphic

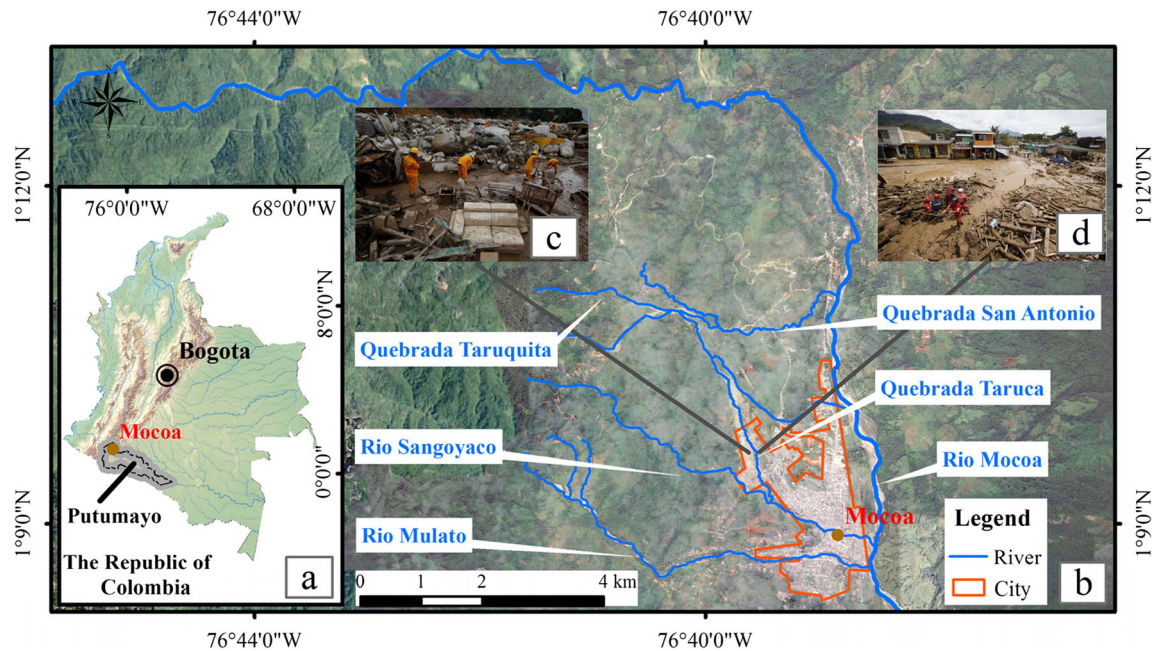


Fig. 1 Location map of Mocoa and photographs of massive debris and mud piled up in the city (source: www.news.cn). (a) Mocoa, identified as a brown dot, is a mountainous city in the Andes located in the northwest of Putumayo. (b) The position relationship between Mocoa and several main rivers. (c, d) Disaster photographs

development into three stages—young stage (HI greater than 0.6), mature stage (HI between 0.35 and 0.60), and old stage (HI less than 0.35). When calculating an HI value, contour i is chosen as a reference, the whole watershed area is assumed to be A , and the area above the contour of the basin is a_i . The height difference between the contour and the lowest point of the basin is h_i , and the height difference between the highest and lowest points is H . The variables are set as

$$x_i = a_i/A \quad (1)$$

$$y_i = h_i/H \quad (2)$$

where x_i is the area percentage based on contour i , and y_i is the percentage of relative height difference.

The points (x_i, y_i) in the rectangular coordinate system are spread to form a curve. It can be defined as

$$y = f(x) \quad (3)$$

On this basis, the definite integral value in the range of 0 to 1 is calculated, and it is HI.

$$HI = \int_0^1 f(x) dx \quad (4)$$

Using DEM data of the watershed and the HI calculation method, the hypsometric integral curve was constructed in Fig. 3 and HI was calculated to be 0.49. According to the HI-based geomorphic development stages proposed by Strahler, and the summary of many watershed hypsometric integral curves (Singh et al. 2008; Xiang et al. 2015), the geomorphic development in Fig. 3 is divided

into three stages and differentiated by the concave and convex curves. The area above convex curve is treated as the young stage; the area below the concave line is considered as the old stage; the area between two lines is known as the mature stage. In the current study, the watershed basin belongs to the mature stage. In the infancy and mature periods, the solid content of the gully is rich, and the HI value is high (Xiang et al. 2015). Therefore, mature-stage Mocoa watershed has a susceptible geomorphic environment for debris flows.

Data source

Pre-disaster and post-disaster images were obtained from different satellite remote sensing companies. The pre-disaster image (Fig. 4(a)) was acquired by the Chinese GF-2 satellite on 15 April 2015 with a 1-m resolution, and the post-image (Fig. 4(b)) was acquired by the American GeoEye-1 satellite on 10 April 2017 with a 0.5-m resolution. Both images have a closed seasonal phase in order to make a comparative analysis. By doing a comparative analysis of the pre-disaster and post-disaster images, it was found that the Mocoa disaster was the result of flood overflowing six rivers: the Rio Mocoa River, the Rio Mulato River, the Rio Sangoyaco River, the Quebrada Taruca River, the Quebrada San Antonio River, and the Quebrada Taruquita River (Fig. 4(c)). The Quebrada Taruca River has two distributaries that would be distinguished using flow directions (north-south, west-east) in this paper.

Disaster characteristics

Mountain hazard distribution

The provenance of this disaster mainly has two sources: river upstream landslides and channel substance erosion. Upstream landslides could provide debris source for the formation of mountain torrents (Sohn et al. 1999, Pierson 2005). Channel substance erosion could provide the debris source for the late debris flow

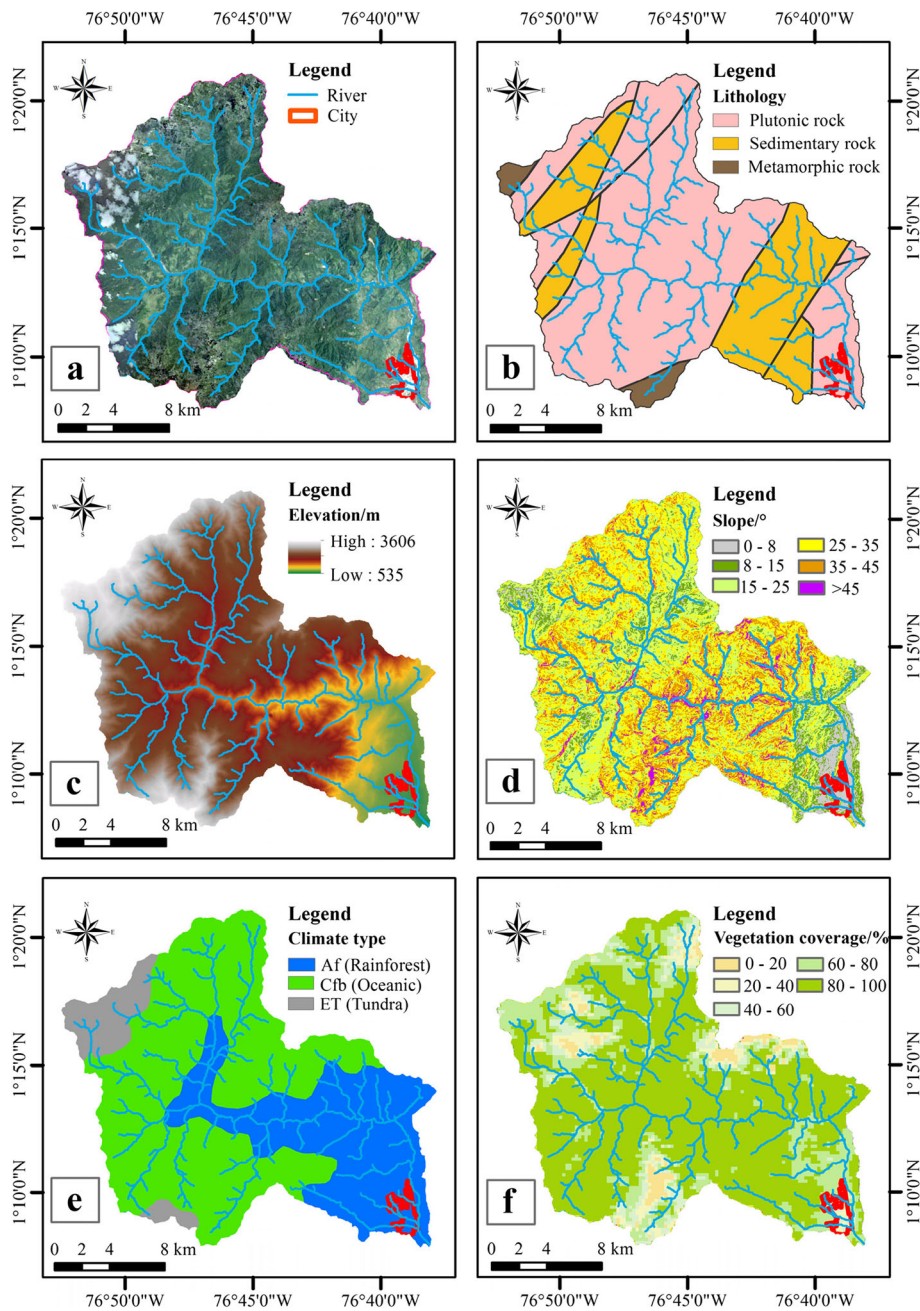


Fig. 2 Mocoa upstream basin characters: (a) image, (b) geology, (c) elevation, (d) slope, (e) climate, and (f) vegetation coverage

evolution occurring along the Quebrada Taruca River (north-south). By using the high-resolution remote sensing images to interpret landslides, 763 landslides around Mocoa were interpreted (Fig. 5(a)); 250 landslides among them were distributed near rivers, and could directly provide debris into rivers. Area percentages of landslides along different rivers were calculated for comparison (Fig. 5(f)). The result shows that the Quebrada Taruca River, the Rio Sangoyaco River, and the Quebrada Taruquita River may have accepted more landslide debris sources. In the Taruca ravine of the Quebrada Taruca River (north-south), the mountain torrents overflowed and evolved into debris flows. Flood overflow areas along different rivers were marked in Fig. 5(a). It could be seen that the major affected areas were mainly distributed along the

Quebrada Taruca River (north-south). The interpretation features of different mountain hazards in the high-resolution remote sensing image were marked (Fig. 5(b-e)).

Mountain hazard chains and compound mountain hazards

Small-scale geo-hazards, such as floods, debris flows, shallow landslides, and landslide lakes, are able to be attributed to and converged into a large-scale single disaster event (Chen et al. 201b). The disaster that occurred in Mocoa could be seen as a consequence of compounded mountain hazards, including landslides, floods, and debris flows (Fig. 6). Different hazards in different places are connected to each other through the mountain hazard chain that could amplify the disaster's effects (Cui and Jia 2015). In this disaster event,

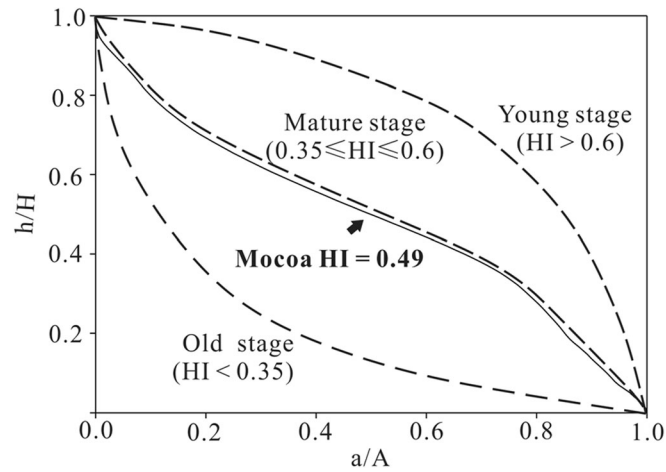


Fig. 3 Hypsometric integral curve. The dotted line represents the three stages of the development of the geomorphology (Singh et al. 2008; Xiang et al. 2015)

heavy rainfalls induced landslides and mountain torrents. Provenance landslides and channel erosion provided debris sources for mountain torrents. Along the Quebrada Taruca River (North-south), debris flows occurred since large amounts of soil were scoured into the water. The model of compound mountain hazards and cascading hazards is illustrated in Fig. 6.

Damage features

Mud and water extent were detected using the satellite images, and damage situations of houses and main roads were obtained (Fig. 7). Disaster damage situations were divided into three categories: washed away, buried, and silted. Damage situation statistics were calculated (Tables 1 and 2). In this disaster event, 12.48 km of main roads is potentially affected, and approximately 1768 buildings were situated within areas that experienced floods or debris flows.

Causal factors

El Niño and La Niña

El Niño and La Niña events are irregular periodic variations of sea surface temperatures and atmospheric pressure over the

tropical eastern Pacific Ocean. The warming phase is known as *El Niño*, and the cooling phase is known as *La Niña*. The circulation of cold and warm phases is a global scale climate oscillation. Extreme climates in Amazonia are linked to El Niño conditions in the tropical Pacific, to sea surface temperature (SST) anomalies in the tropical Atlantic, or to a combination of both. The impacts during most El Niño events include below-average rainfall over Indonesia and northern South America and above average rainfall in southeastern South America, eastern equatorial Africa, and the southern USA (Barnston 2014). The strongest shifts of El Niño and La Niña remain fairly consistent in the regions and seasons shown on the maps (Fig. 8(a, b)).

Usually, La Niña could bring more rainfall and El Niño bring drought to the Amazon Basin. Poorer rainy seasons even occurred during El Niño events, while wetter than average conditions were also observed during La Niña years (Alencar et al. 2006, Moeletsi et al. 2011, Pereira et al. 2013). These two phenomena have obvious effects in regions that have dry and rainy seasons. A major El Niño event was recorded in the years from 2014 to 2016 (Fig. 8(c)).

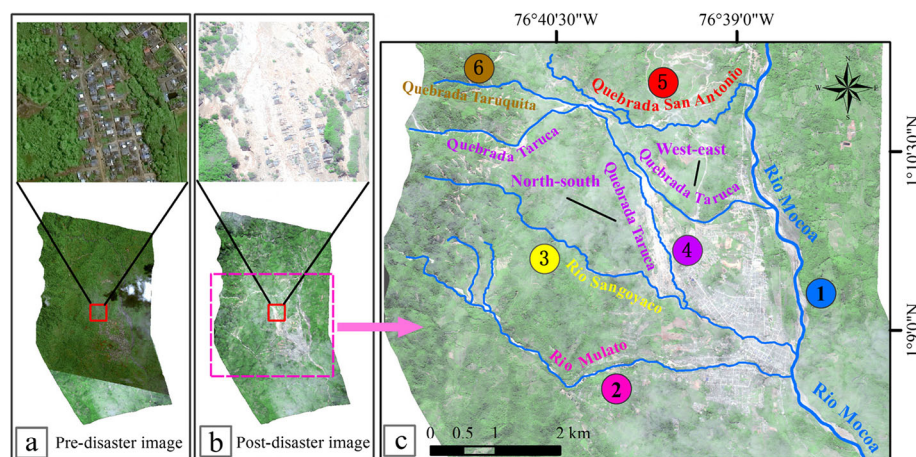


Fig. 4 Remote sensing images of pre-disaster and post-disaster. (a) Pre-disaster image (April 15, 2015). (b) Post-disaster image (April 10, 2017). (c) Overflowing rivers: ① the Rio Mocoa River, ② the Rio Mulato River, ③ the Rio Sangoyaco River, ④ the Quebrada Taruca River (two branches downstream: north-south, west-east), ⑤ the Quebrada San Antonio River, and ⑥ the Quebrada Taruquita River

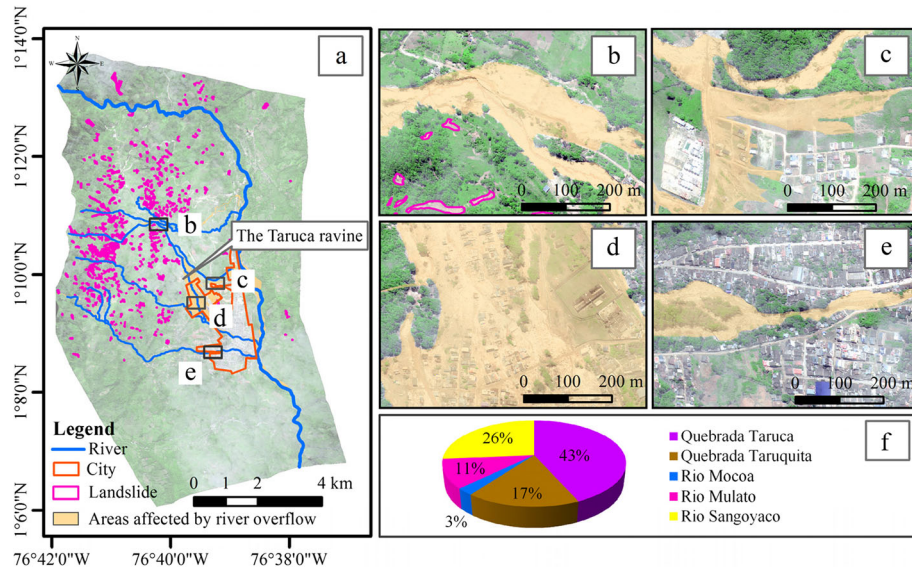


Fig. 5 Remote sensing image characteristics. (a) Distribution of landslides. (b) Flood channel erosion of the Quebrada Taruca River. (c) Flood overflow of the Quebrada San Antonio River. (d) Debris flow’s erosion and deposits the Quebrada Taruca River. (e) Flood overflow of the Rio Mulato River. (f) Area percentage of landslides along different rivers. The flood channel erosion will scour the river banks and widen the river. Flood overflow generally does not change the width of the river, and it often submerges the area surrounding the river. Water stains are left after the flood recedes. The debris flow’s erosion and deposits are very destructive to buildings, and a large number of houses were destroyed and buried

Rainfall

Inter-annual rainfall change

During an El Niño event, droughts could occur virtually anywhere in the world (NDMC 2017). Northeastern South America from Brazil up to Venezuela showed one of the strongest relationships (Ropelewski and Halpert 1987). In 17 El Niño events, this region had 16 dry episodes. The Standardized Precipitation-Evapotranspiration Index (SPEI) is a drought index that can measure drought severity using monthly mean temperatures, monthly precipitation, monthly sunshine hours (Vicenteserrano et al. 2010), and the intensity of the drought (Abdullah 2014). SPEI was classified in Table 3. In the years 2014–2016, there was a major El Niño event. A sharp drop of rainfall caused the long-time moderately

and severe drought ($-2 < \text{SPEI} \leq -1$) (Fig. 9). By the second half of 2016, a La Niña event began to appear, and it was followed by increased rainfalls.

Antecedent rainfall

This pre-disaster period of 2017 had unusual precipitation: 184 mm in January, 198 mm in February, and 166 mm in March (World Weather Online 2017). Antecedent rainfalls over several days before these disasters made the soil abnormally saturated, making it easier to slide and flow. A sudden increase in rainfall (Fig. 10) occurred on 1 April, and the terrain effect enhanced the rainfall’s effects. The abundant water yield coming from antecedent precipitation met this rainfall and developed into floods. Heavier rainfalls on the event night became “the last straw” of this disaster.

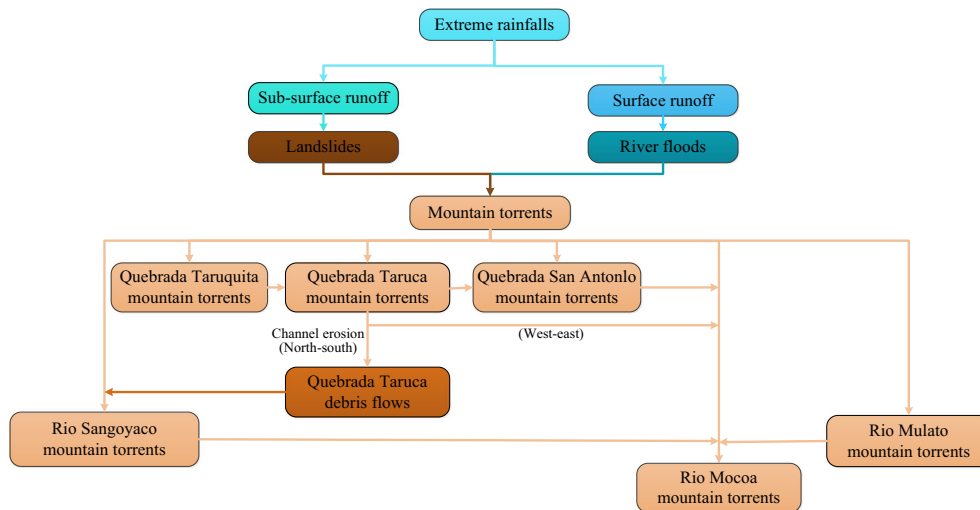


Fig. 6 The model of compound mountain hazards occurring in Mocoa

Recent Landslides

Table 1 Damage situation subjected to roads (no field validation)

Objects	Damage situation	Characteristics	Length (m)
Roads	Washed away	Completely destroyed and almost disappeared	5979.40
	Buried	Deposited by a large amount of sediment	1191.97
	Silted	Deposited by a small amount of sediment	5308.64

Table 2 Damage situation subjected to buildings (no field validation)

Objects	Damage process	Characteristics	Number
Buildings	Washed away	Completely destroyed and almost disappeared	288
	Buried	Filled with mud sediment, but frames remained	505
	Silted	Deposited by a small amount of sediment	975

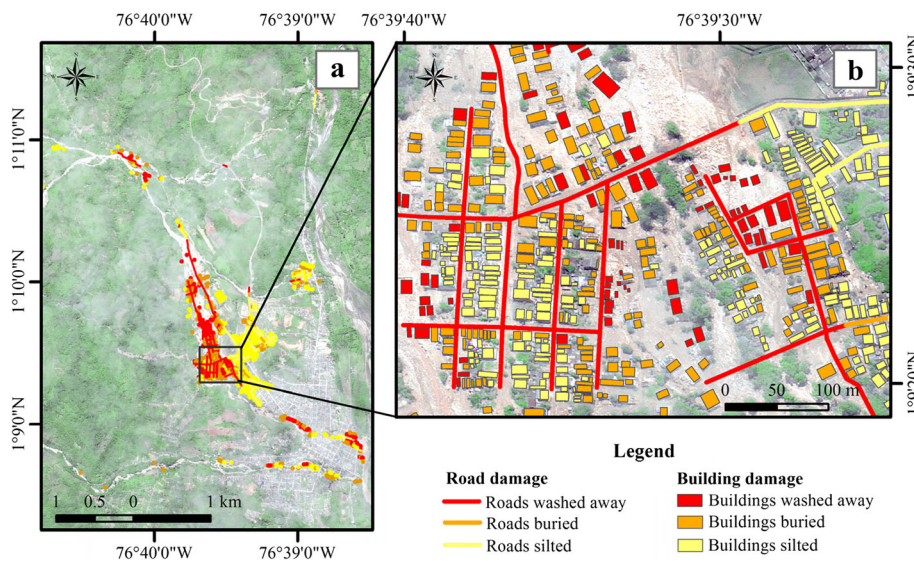


Fig. 7 Post-disaster damage situations of buildings and roads. (a) Damage overview. (b) Partial enlarged detail of post-disaster damage characteristics

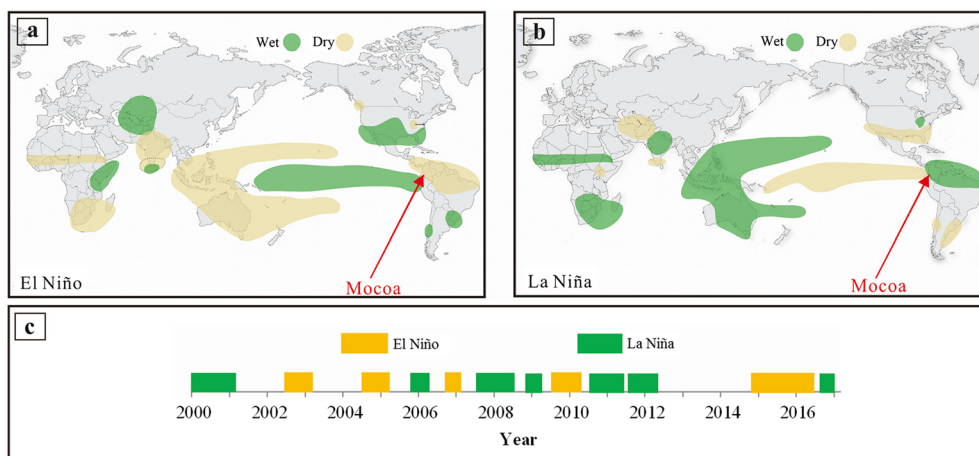


Fig. 8 The influence of El Niño and La Niña on Mocoa. (a, b) Rainfall affected by El Niño and La Niña (Ropelewski and Halpert 1989, Mason and Goddard 2011, Barnston 2014, modified from IRI 2014). (c) A timeline that records the El Niño and La Niña events between 2000 and March 2017

Table 3 SPEI class

Range	Condition
$SPEI \leq -2$	Extreme drought
$-2 \leq SPEI \leq -1.5$	Severe drought
$-1.5 \leq SPEI \leq -1$	Moderately drought
$-1 \leq SPEI \leq 1$	Near normal
$1.0 \leq SPEI \leq 1.5$	Moderately wet
$1.5 \leq SPEI \leq 2$	Severely wet
$2 \leq SPEI$	Extremely wet

Cui et al. (2007) proved the different contributions of antecedent precipitation including IAP (indirect antecedent precipitation), DAP (direct antecedent precipitation), and TP (triggering precipitation) using debris flow cases occurring in the Jiangjia Ravine, China. TP defines the short-duration precipitation that stimulates the occurrence of debris flows. DAP directly affects the water content of solids and takes part in the formation of debris flows. Unlike DAP and TP, the effect of IAP mainly changes the soil moisture through a long accumulation period and influences the intensity and quantity of rainfall necessary to trigger debris flows. The research showed that the contributions of IAP and DAP to debris flows were 44% while the triggering precipitation (1 h intensity) contributed only 37% (Cui et al. 2007). Debris flows are initiated under the integrated impacts of TP, DAP, and IAP. When calculating the IAP value, it is defined as

$$IAP = \sum_{i=1}^n \left(P_i \prod_{j=1}^i K_j \right) \tag{5}$$

In the above formula, P_i is the daily precipitation (mm) from the first day ($i = 1$) to the preceding n days ($i = n$), i and j both state the number of days before the start of the rainfall process triggering the hazards, and K_j is a decay coefficient in j^{th} day's weather condition due to evaporation. K_j is the key to calculate IAP, but different places may have different decay coefficients due to evaporation differences. Research about the evapotranspiration of a tropical rain forest in central Amazonia was performed by Leopoldo et al. (1995). Taking this research into consideration, 0.87 and 1 were

chosen as the decay coefficient in the cloudy day or sprinkle day, and the decay coefficient in the rain day, total 20 days (from 5 to 24 March) were chosen in current calculation ($n = 20$). The rainfall process indicated that the precipitation started on 25 March and the hazards occurred on 1 April. The peak rainfall immediately before the incident was 6.1 mm which is considered as TP. The DAP can be calculated, using formula 6, by simply summing the rainfall from 25 March until preceding TP.

$$DAP = \sum_{k=1}^m P_k \tag{6}$$

In the above formula, P_k is the daily precipitation (mm), m is the number of total rain days from the beginning of rainfall to the occurrence of disasters, k is the number of rain days from the start of rain. Here, the total 7 days (from 25 to 31 March) were chosen in current calculation ($m = 7$). Depending on the relationship and the calculation method of IAP, DAP, and TP, their values were obtained separately. The rainfall contributing to hazard occurrence was the summation of IAP, DAP, and TP and calculated as 101.1 mm in which TP contributed 6.1 mm, DAP contributed 23.8 mm, and IAP was 71.2 mm.

Vegetation coverage change

Using the same method as Fig. 2(f), the vegetation coverages at the interval of 2 years from 2000 to 2016 were calculated using NDVI data from June to August. From several years of vegetation coverage conditions, a significant change (Fig. 11) could be found. The 2010 and 2012 vegetation conditions of the Mocoa watershed were in a better condition, while 2014, 2016, and 2017 were poorer. The corrosion inhibition effect of the vegetation canopy is realized on the interception of precipitation and the reduction of raindrop energy. It can weaken the kinetic energy of raindrops. Vegetation plays an important role in the control of debris flows by adjusting soil moisture through evapotranspiration and intercepting rainfall (Li and Clarke 2007).

In recent years, vegetation coverages of this Mocoa watershed have remained poor, which would reduce its ability to cope with heavy rainfalls. In the seasonal parts of the South American Amazon forest, foliage growth and coverage vary between the dry and wet seasons (Mongabay 2007; Myneni et al. 2007). This

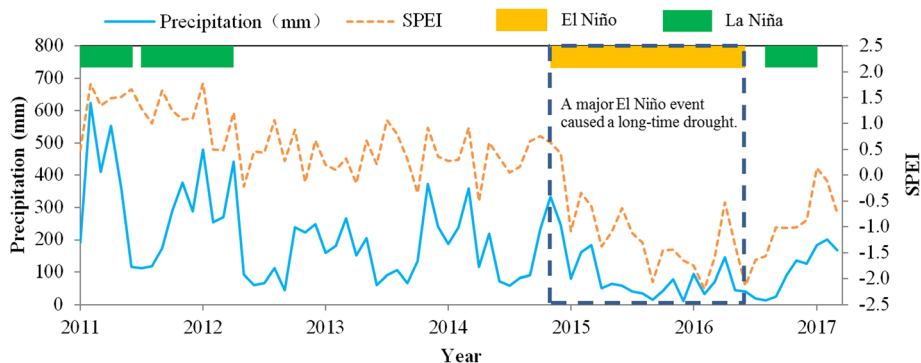


Fig. 9 Rainfall amount (2011- March 2017) in Mocoa, Putumayo (World Weather Online 2017)

Recent Landslides

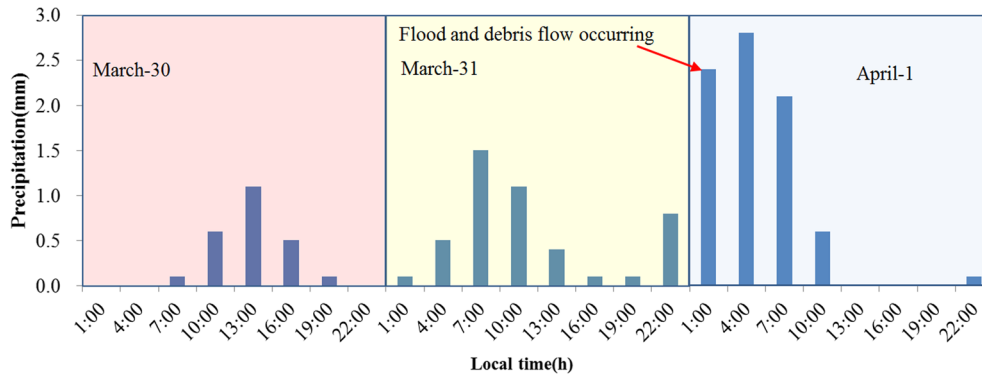


Fig. 10 Rainfall during the period from March 30 to April 1, 2017, in Mocoa (World Weather Online 2017). Rainfall increased in the early morning of April 1, 2017. It should also be noted that the mountain effect around Mocoa would increase rainfall. The records of the rainfall station can be used as a reference for the rainfall trend

phenomenon illustrates the importance of water to rainforests. Taking into account the impacts of El Niño and La Niña, a relationship between average vegetation coverages and the occurrence of El Niño and La Niña was built (Fig. 12). The 2014–2016 El Niño event was among the strongest on record. The decrease of precipitations affected the growth of vegetation in this watershed.

vegetation coverage reduces the interception and water holding capacities that are responsible for this incident.

Discussion and conclusion

Through the interpretation of remote sensing images, this study obtained rich information about mountain hazard distributions,

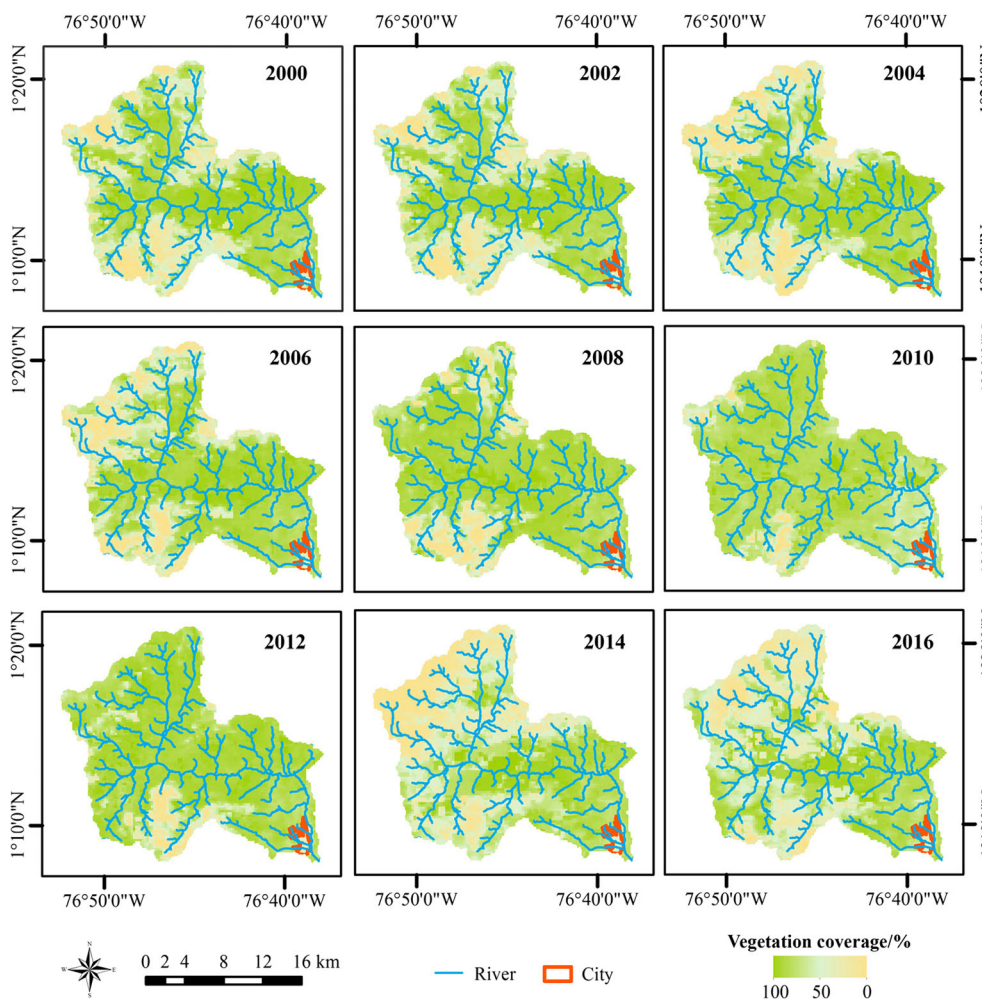


Fig. 11 Variation of vegetation coverage

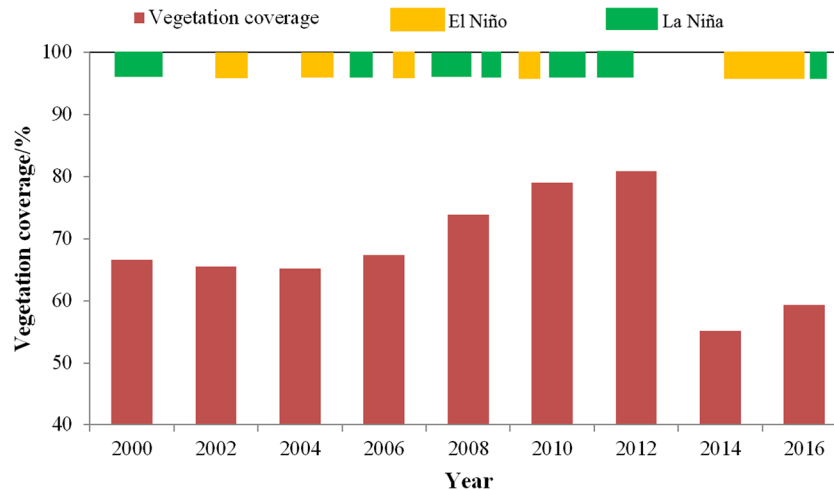


Fig. 12 The relationship between vegetation coverage and a timeline of El Niño and La Niña

hazard chains, compound hazards, and damage features. This research shows that the Mocoa disaster was the comprehensive result of landslides, mountain torrents, and debris flows. As a typical compound disaster, the Mocoa disaster caused great damage. Although heavy rainfalls were the trigger for this disaster, it should be realized that previous droughts also played an important role in this disaster event. In this disaster, the previous El Niño event (2014–2016) needs to be taken into account, particularly since it had an important influence on rainfall and vegetation. The drought caused by the earlier El Niño affected the growth of vegetation. The decreased vegetation coverage reduced the ability of the ecosystem to adjust heavy rainfalls and to protect the earth surface. The later La Niña event brought a large amount of heavy antecedent rainfalls. The continuous rainfalls caused the soil to stay saturated, making mountain hazards triggered by heavy rainfalls more likely.

It is unwise for people to pay attention only to the antecedent rainfalls that trigger mountain hazards and ignore the research on the early climate impact. With the increase of extreme weather events, compound disaster events would also increase, especially in the adequate-rainfall mountainous areas. The research on the climate background is of guiding significance to the formulation of disaster prevention and mitigation plans.

Acknowledgements

The authors are grateful for the financial support from the opening fund of the State Key Laboratory of Hydraulics and Mountain River Engineering (SKHL1609). This research was also supported by the projects of the International partnership program of the Chinese Academy of Sciences (No. 131551KYSB20160002) and the Key Research Program of Frontier Sciences, CAS (No. QYZDY-SSW-DQC006). The authors would also like to thank the theme-based research grant (T22-603/15-N) and the general research fund (16209717) provided by the Research Grants Council of Hong Kong. The authors are also grateful for the financial sponsorship from the National Natural Science Foundation of China (51709052) and the support of the HKUST Jockey Club Institute for Advanced Study. The authors would like to thank the support of the HKUST Jockey Club Institute for Advanced Study and the financial support by the Hong Kong Jockey Club Disaster Preparedness and Response Institute (HKJCDPR18EG01) and the Hong Kong Jockey Club Charities Trust.

Open Access This article is distributed under the terms of the Creative Commons Attribution 4.0 International License (<http://creativecommons.org/licenses/by/4.0/>), which permits unrestricted use, distribution, and reproduction in any medium, provided you give appropriate credit to the original author(s) and the source, provide a link to the Creative Commons license, and indicate if changes were made.

References

- ABC News (2017) Colombia landslide kills more than 250, hundreds injured and missing. <http://www.abc.net.au/news/2017-04-02/colombia-landslide-leaves-more-than-100-dead/8408392> last accessed 11 January 2018
- Abdullah HM (2014) Standardized precipitation evapotranspiration index (SPEI) based drought assessment in Bangladesh. In: Proceedings 5th International Conference on Environmental Aspects of Bangladesh [ICEBA 2014], vol. 23, pp 40–42
- Alencar A, Nepstad D, Diaz MCV (2006) Forest understory fire in the Brazilian Amazon in ENSO and non-ENSO years: area burned and committed carbon emissions. *Earth Interact* 10(6):1–17
- ArcGIS Help (2012) Hydrologic analysis sample applications. <http://resources.arcgis.com/en/help/main/10.1/index.html#//00920000052000000> last accessed 11 Jan 2018
- Barnston A (2014) How ENSO leads to a cascade of global impacts. NOAA *Climate.gov* <https://www.climate.gov/news-features/blogs/enso/how-enso-leads-cascade-global-impacts> last accessed 11 Jan 2018
- Chen XQ, Cui P, Li Y, Zhao WY (2011a) Emergency response to the Tangjiashan landslide-dammed lake resulting from the 2008 Wenchuan Earthquake, China. *Landslides* 8(1):91–98
- Chen YS, Kuo YS, Lai WC, Tsai YJ, Lee SP, Chen KT (2011b) Reflection of typhoon morakot—the challenge of compound disaster simulation. *J Mt Sci* 8(4):571–581
- Cui P, Zhu YY, Chen J, Han YS, Liu HJ (2007) Relationships between antecedent rainfall and debris flows in Jiangjia Ravine, China. In: Chen C, Major JJ (eds) *Debris-flow hazards mitigation: mechanics, prediction, and assessment*. Millpress Science Publisher, Rotterdam, pp 3–10
- Cui Y, Luo Y, Wang L (2011) Extraction of vegetation fraction based on the dimidiate pixel model and vegetation index transform plan. In: Proceedings PIAGENG 2010: Photonics and imaging for agricultural engineering, SPIE, U.S.A., vol. 7752, p 775202
- Cui P (2014) Progress and prospects in research on mountain hazards in China. *Prog Geogr* 33(2):145–152
- Cui P, Jia Y (2015) Mountain hazards in the Tibetan Plateau: research status and prospects. *National Science Review* 2(4):397–399
- Cui YF, Zhou XJ, Guo CX (2017) Experimental study on the moving characteristics of fine grains in wide grading unconsolidated soil under heavy rainfall. *J Mt Sci* 14(3):417–431
- Dai FC, Lee CF (2002) Landslide characteristics and slope instability modeling using GIS, Lantau Island, Hong Kong. *Geomorphology* 42(3):213–228
- Eidenshink JC, Faundeen JL (1994) The 1 km AVHRR global land data set: first stages in implementation. *Int J Remote Sens* 15(17):3443–3462

- Eisbacher GH (1982) Mountain torrents and debris flows. *Episodes* 4:12–17
- Fick SE, Hijmans RJ (2017) Worldclim 2: new 1-km spatial resolution climate surfaces for global land areas. *Int J Climatol* 37(12):4302–4315
- Ge YG, Cui P, Su FH, Zhang JQ, Chen XZ (2014) Case history of the disastrous debris flows of Tianmo Watershed in Bomi County, Tibet, China: some mitigation suggestions. *Journal of Mountain Science* 11(5):1253–1265
- Guardian T (2017) Colombia landslide leaves at least 254 dead and hundreds missing. <https://www.theguardian.com/world/2017/apr/01/colombia-landslide-mocoa-putumayo-heavy-rains> last accessed 11 Jan 2018
- Hughes T (2017) Colombian slide disaster: here's how the 'debris flow' likely occurred. *USA Today* <https://www.usatoday.com/story/news/2017/04/02/colombian-slide-disaster-how-debris-flow-likely-occurred/99954752/> last accessed 11 Jan 2018
- IRI (2014) What changes in rainfall are typical during El Niño? <http://iridl.ldeo.columbia.edu/maproom/IFRC/FIC/elninorain.html> last accessed 11 Jan 2018
- Iverson RM (2000) Landslide triggering by rain infiltration. *Water Resour Res* 36(7):1897–1910
- Leopoldo PR, Franken WK, Nova NAV (1995) Real evapotranspiration and transpiration through a tropical rain forest in central amazonia as estimated by the water balance method. *For Ecol Manag* 73(1):185–195
- Lévy S, Jaboyedoff M, Locat J, Demers D (2012) Erosion and channel change as factors of landslides and valley formation in Champlain Sea Clays: the Chacoura River, Quebec, Canada. *Geomorphology* 145:12–18
- Li G, Clarke D (2007) Vegetation patterns and the prediction of debris flow. In: Chen C, Major JJ (eds) *Debris-flow hazards mitigation: mechanics, prediction, and assessment*. Millpress Science Publisher, Rotterdam, pp 35–44
- Mason SJ, Goddard L (2001) Probabilistic precipitation anomalies associated with ENSO. *Bull Am Meteorol Soc* 82(4):619–638
- Moeletsi ME, Walker S, Landman WA (2011) ENSO and implications on rainfall characteristics with reference to maize production in the Free State Province of South Africa. *Phys Chem Earth, Parts A/B/C* 36(14):715–726
- Mongabay (2007) Amazon rainforest does have rainy and dry seasons. <https://news.mongabay.com/2007/03/amazon-rainforest-does-have-rainy-and-dry-seasons/> last accessed 11 Jan 2018
- Myneni RB, Yang W, Nemani RR, Huete AR, Dickinson RE, Knyazikhin Y (2007) Large seasonal swings in leaf area of Amazon rainforests. *Proc Natl Acad Sci U S A* 104(12):4820–4823
- NASA (2017) LAADS DAAC. <https://ladsweb.modaps.eosdis.nasa.gov/search/order/2/MOD13Q1-6> last accessed 11 Jan 2018
- NDMC (2017) ENSO and drought forecasting. <http://drought.unl.edu/DroughtBasics/ENSOandForecasting.aspx> last accessed 11 Jan 2018
- OneGeology (2007) One geology providing geoscience data globally. <http://portal.onegeology.org/OnegeologyGlobal/> last accessed 11 Jan 2018
- Peel MC, Finlayson BL, McMahon TA (2007) Updated world map of the Köppen-Geiger climate classification. *Hydrol Earth Syst Sci Discuss* 4(2):439–473
- Pereira LCC, Oliveira SMOD, Costa RMD, Costa KGD, Vila-Concejo A (2013) What happens on an equatorial beach on the Amazon coast when La Niña occurs during the rainy season? *Estuar Coast Shelf Sci* 135:116–127
- Pierson TC (2005) Hyperconcentrated flow—transitional process between water flow and debris flow. In: *Debris-flow hazards and related phenomena*, Springer, Berlin, pp 159–202
- Preuth T, Glade T, Demoulin A, Glade T, Crozier MJ (2010) Stability analysis of a human-influenced landslide in eastern Belgium. *Geomorphology* 120(1):38–47
- Reliefweb (2017) Colombia—inundaciones en Mocoa, Putumayo - Reporte de Situación No 03 (al 11042017) <http://reliefweb.int/report/colombia/colombia-inundaciones-en-mocoa-putumayo-reporte-de-situaci-n-no-03-al-11042017> last accessed 11 Jan 2018
- Ropelewski CF, Halpert MS (1987) Global and regional scale precipitation patterns associated with the El Niño/Southern Oscillation. *Mon Weather Rev* 115(8):1606–1626
- Ropelewski CF, Halpert MS (1989) Precipitation patterns associated with the high index phase of the Southern Oscillation. *J Clim* 2(3):268–284
- Runyan CW, D'odorico P (2014) Bistable dynamics between forest removal and landslide occurrence. *Water Resour Res* 50(2):1112–1130
- Semana (2017) Tragedia en mocoa: Cientos de víctimas por avalancha. <http://www.semana.com/nacion/multimedia/tragedia-en-mocoa-sub-e-el-numero-de-muertos-por-la-avalancha/520522> last accessed 11 Jan 2018
- Sillitoe RH, Jaramillo L, Castro H (1984) Geologic exploration of a molybdenum-rich porphyry copper deposit at mocoa, Colombia. *Econ Geol* 79(1):106–123
- Singh O, Sarangi A, Sharma MC (2008) Hypsometric integral estimation methods and its relevance on erosion status of north-western lesser Himalayan watersheds. *Water Resour Manag* 22(11):1545–1560
- Sohn YK, Rhee CW, Kim BC (1999) Debris flow and hyperconcentrated flood-flow deposits in an alluvial fan, northwestern part of the Cretaceous Yongdong Basin, Central Korea. *J Geol* 107(1):111–132
- Stow DA, Hope A, McGuire D, Verbyla D, Gamon J, Huemmrich F (2004) Remote sensing of vegetation and land-cover change in Arctic Tundra Ecosystems. *Remote Sens Environ* 89(3):281–308
- Strahler AH (1952) Hypsometric (area-altitude) analysis of erosional topography. *Geol Soc Am Bull* 63(11):1117–1142
- USGS (2017) Global data explore. <https://gdex.cr.usgs.gov/gdex/> last accessed 11 Jan 2018
- Vicenteserrano SM, Beguería S, Lópezmoreno JI (2010) A multiscalar drought index sensitive to global warming: the standardized precipitation evapotranspiration index. *J Clim* 23(7):1696–1718
- Wang NQ, Yong Y (2008) Characteristics and mechanism of landslides in loess during freezing and thawing periods in seasonally frozen ground regions. *Journal of Disaster Prevention and Mitigation Engineering* 28(2):163–166
- World Weather Online (2017) Mocoa, putumayo monthly climate average, colombia <https://www.worldweatheronline.com/mocoa-weather-averages/putumayo/co.aspx> last accessed 11 Jan 2018
- Xiang LZ, Li Y, Chen HK, Su FH, Huang X (2015) Sensitivity analysis of debris flow along highway based on geomorphic evolution theory. *Resour Environ Yangtze Basin* 24(11):1984–1992 (in Chinese)
- Yang L, Meng X, Zhang X (2011) SRTM DEM and its application advances. *Int J Remote Sens* 32(14):3875–3896
- Yilmaz AG (2017) Climate change effects and extreme rainfall non-stationarity. In: *Proceedings Institution of Civil Engineers—water management*, Thomas Telford Ltd, United Kingdom, vol. 170, pp 57–65
- Zhou JW, Cui P, Yang XG, Su ZM, Guo XJ (2013) Debris flows introduced in landslide deposits under rainfall conditions: the case of Wenjiagou gully. *J Mt Sci* 10(2):249–260
- Zhou JW, Cui P, Hao MH (2016) Comprehensive analyses of the initiation and entrainment processes of the 2000 Yigong catastrophic landslide in Tibet, China. *Landslides* 13(1):39–54
- Zhu S, Tang G, Li F, Xiong L (2013) Spatial variation of hypsometric integral in the loess plateau based on DEM. *Acta Geograph Sin* 68(7):921–932

D. Cheng · F. Su · Y. Jia

Key Laboratory of Mountain Hazards and Earth Surface Process, Chinese Academy of Sciences, Chengdu, 610041, China

D. Cheng

e-mail: chengdq90@imde.ac.cn

F. Su

e-mail: fhsu@imde.ac.cn

Y. Jia

e-mail: 8394186@163.com

D. Cheng · F. Su · Y. Jia

Institute of Mountain Hazards and Environment, Chinese Academy of Sciences, Chengdu, 610041, China

D. Cheng · Y. Jia

University of Chinese Academy of Sciences, Beijing, 100049, China

Y. Cui (✉) · C. E. Choi

Department of Civil and Environmental Engineering, The Hong Kong University of Science and Technology, Clear Water Bay, Hong Kong, China
Email: yifeicui@ust.hk

C. E. Choi

The HKUST Jockey Club Institute for Advanced Study, The Hong Kong University of Science and Technology, Clear Water Bay, Kowloon, Hong Kong